The effect of gain medium length on dynamic mode stability in semiconductor lasers with a long intra-cavity filter

Oh Kee Kwon,[1,*] Chul Wook Lee,[1] Jang Wook Shin,[1] Eun Deok Sim,[1] Jong-Hoi Kim[1], Dong Hun Lee,[1] Dong Soo Bang,[2] and Yong Soon Baek,[1]

[1]RF and Optical Devices Department, IT Convergence and Components Laboratory, Electronics and Telecommunications Research Institute (ETRI), Daejeon, 305-350, Korea
[2]Novatronix corp. NovaBldg, 641-3, Yeoksam-dong, Gangnam-gu, 135-909, Seoul, Korea
[*]okkwon@etri.re.kr

Abstract: We investigate theoretically and experimentally the effect of the physical length of gain medium on dynamic mode stability in semiconductor lasers with an intra-cavity filter. In simulation, two types of analysis models were used to examine the lasing properties and to analyze the dynamic mode stability of the external-cavity system, respectively. In experiment, two different kinds of the structures were fabricated and their spectra were analyzed. Both simulation and measurement results show clearly the length of the gain medium has a critical influence on the stability around the peak wavelength of the filter.

OCIS codes: (140.3410) Laser resonators, (230.3120) Integrated optics devices.

References and links

1. M. Zirngibl, B. Glance, L. W, Stulz, C.H. Joyner, G. Raybon, and I. P. Kaminow, "Characterization of a multiwavelength waveguide grating router laser," IEEE Photon. Technol. Lett. **6,** 1082-1084 (1994).
2. C. H. Joyner, C. R. Doerr, L. W. Stulz, M. Zirngibl, and J. C. Centanni, "Low-threshold nine-channel waveguide grating router-based continuous wave transmitter," J. Lightwave Technol. **17,** 647-651 (1999).
3. J. B. D. Soole, K. R. Poguntke, A. Scherer, H. P. LeBlanc, C. Chang-Hasnain, J. R. Hayes, C. Caneau, R. Bhat, and M.A. Koza, "Wavelength-selectable laser emission from a multistripe array grating integrated cavity laser," Appl. Phys. Lett. **61,** 2750-2752 (1992).
4. O. K. Kwon, J. H. Kim, K. H. Kim, E. D. Sim, and K. R. Oh, "Widely tunable multichannel grating cavity laser," IEEE Photon. Tech. Lett. **18**, 1699-1701 (2006).
5. C. E. Zah, F. J. Facire, B. Pathak, R. Bhat, C. Caneau, P. S. D. Lin, A. S. Gozdz, N. C. Andreadakis, M. A. Koza, and T. P. Lee, "Monolithic integration of multiwavelength compressive-strained multiquantum-well distributed feedback laser array with star coupler and optical amplifiers," Electron Lett. **28**, 2361-2362 (1992).
6. D. F. Welch, F. A. Kish, S. M. R. Nagarajan, M. Kato, C. H. Joyner, J. L. Pleumeekers, R. P. Schneider, J. Bäck, A. G. Dentai, V. G. Dominic, P. W. Evans, M. Kauffman, D. J. H. Lambert, S. K. Hurtt, A. Mathur, M. L. Mitchell, M. Missey, S. Murthy, A. C. Nilsson, R. A. Salvatore, M. F. Van Leeuwen, J. Webjorn, M. Ziari, S. G. Grubb, D. Perkins, M. Reffle, and D. G. Mehuys, "Large-scale InP photonic integrated circuits: enabling effect scaling of optical transport networks," IEEE J. Sel. Top. Quantum Electron. **13,** 22-31 (2007).
7. C. R. Doerr, "Theoretical stability analysis of side-mode operation in uncontrolled mode-selection semiconductor lasers," IEEE Photon Technol. Lett. **9**, 1457-1459 (1997).
8. L. Möller, C. R. Doerr, C. H. Joyner, and M. Zirngibl, "Mode stabilization technique for the multifrequency laser," *in Proceedings of the Optical Fiber Communication and Conference*, Paper TuL4-1-TuL4-3 (2000).
9. J. H. den Besten, R. G. Broeke, M. van Geemert, J. J. M. Binsma, F. Heinrichsdorff, T. van Dongen, E. A. J. M. Bente, X. J. M Leijtens, and M. K. Smit, "An integrated 4×4-channel multiwavelength laser on InP," IEEE Photon. Technol. Lett. **15,** 368-370 (2003).
10. M. H. Kwakernaak, W. K. Chan, N. Maley, H. Mohseni, L. Yang, D. R. Capewell, B. Kharas, V. Frantz, T. Mood, G. A. Pajer, D. A. Ackerman, J. G. Kim, and D. H. Lee, "Multi-frequency laser monolithically integrating InGaAsP gain elements with amorphous silicon AWG," *in Proceedings of the Optical Fiber Communication and Conference*, Paper OWH4 (2006).
11. E. Detoma, B. Tromborg, and I. Montrosset, "The complex way to laser diode spectra: example of an external cavity strong optical feedback," IEEE J. Quantum Electron. **41,** 171-182 (2005).

#118015 - $15.00 USD Received 1 Oct 2009; revised 8 Nov 2009; accepted 16 Nov 2009; published 30 Nov 2009

12. H. Ghafouri-Shiraz, *Distributed feedback laser diodes and optical tunable filters,* (John Wiley & Sons Ltd, England, 2003).
13. M. H. Kwakernaak, W. Chan, D. Capewell, V. Frantz, D. Kharas, A. Ulmer, T. Petrova, R. Farkas, D. Ackerman, T. Mood, and J. G. Kim, "a-Si integrated photonics: phase II final report prepared for Dewell Elecom Inc.," *Sanroff corp., 201 Washington Road Princeton, N.J. 08543* (2005).
14. R. J. Lang, A. Yariv, "Intermodal stability of a coupled-cavity semiconductor laser," IEEE J. Quantum Electron. **QE-22,** 631-636 (1986).

1. Introduction

Long-cavity multi-channel laser (MCL) uses an array of semiconductor optical amplifiers (SOAs) on one side or both sides of a wavelength selective element (WSE) such as arrayed waveguide grating (AWG) [1, 2] or concave grating (CG) [3, 4]. The WSE acts as an intra-cavity filter and the lasing wavelength is selected by turning on the appropriate channel in the SOA array. The channel spacing is adjusted by controlling the linear dispersion of the WSE and is typically very accurate. However, compared to the short cavity MCL such as an array of integrated DFB lasers combined with a star coupler [5] or a multiplexer [6], the modulation speed is limited by the long cavity, and moreover, since the mode spacing corresponding to the total cavity is much narrower than the WSE passband, many longitudinal modes exist within the passband width.

As for the longitudinal mode stability, the most important feature in long-cavity lasers, it has been shown experimentally stable single mode operation can be achieved even if passband width contains many modes and also theoretically reported that to maximize the stability both the cavity length and the passband width must be minimized [7]. Still, it is practically difficult to minimize these two parameters at the same time because narrowing the passband can make the AWG larger and thus the cavity longer. Besides, since linewidth enhancement factor and internal reflection between the gain and passive sections are usually uncontrollable parameters, it is not easy to find the method for improving the mode stability further in this type of laser without the use of additional filters [8], [9].

On the other hand, a novel multi-frequency laser monolithically integrating InGaAsP gain sections with index matched amorphous silicon (a-Si) waveguide has been reported recently [10]. It is expected to be a low-cost photonic integrated device because it can be easily implemented by using PECVD-based technology without the need for multiple epitaxial growths. However, the device seriously suffered from the mode instability and showed the multimode operation in spite of the proper design (-3 dB AWG passband width of about 0.6 nm and cavity length of about 1.2 cm), compared to the other structures [1]-[4].

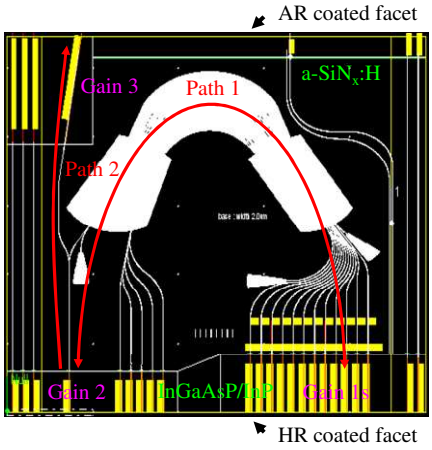

Fig. 1. (a) Design layout of the MCL. a-SiN_x:H denotes a hydrogenated amorphous silicon nitride.

#118015 - $15.00 USD Received 1 Oct 2009; revised 8 Nov 2009; accepted 16 Nov 2009; published 30 Nov 2009

In order to examine the cause of this phenomenon theoretically and experimentally, we first simulated the dynamic mode stability of the device based on the external-cavity laser model with frequency-filtered feedback [11] and then fabricated it with some modifications in design and fabrication from its original structure. In this paper, we present some simulation and measurement results showing the large contribution to the mode stability in the long-cavity lasers with an intra-cavity filter.

2. Analysis models and simulation results

Figure 1 shows a design layout of the device which consists of InGaAsP gain sections, amorphous silicon (a-Si) waveguides (WGs), an a-Si AWG, and an a-Si Y-branch WG monolithically integrated on a single InP substrate. The laser cavity (path1) is formed between the HR-coated facets of one of the gain sections on the right (gain 1) and the common gain section (gain 2). Part of the light is branched out of the cavity (path 2) and amplified through an output amplifier (gain 3).

Two types of the structures were introduced in order to analyze the operational properties of the device as shown in Fig. 2. The first structure realistically describing the device structure in detail provides the information about lasing properties, power distributions across the cavity, and the contributions of the path 2 to the path 1. The structure was modeled by using a well-known transfer matrix method (TMM) including the carrier rate equation [12]. The laser and a-Si waveguide parameters were extracted from the measured data [13] of the ridge MQW laser diodes (ridge width = 2μm) for the integration, a-Si rib WGs (width = 2 μm), and a-Si AWGs. Numerical simulations have been done for the [9] with the parameters listed in Table I. Simulation results such as L-I characteristics were good agreement with the measured data. Figure 3 shows the calculated normalized power distributions of the lasing mode with the lowest threshold gain along the path 1 under the current condition 1 (threshold, $I_{G1}/I_{G2}/I_{G3}$ = 38.6/38.6/0mA, solid lines) and the condition 2 (80/60/0mA, dashed lines).

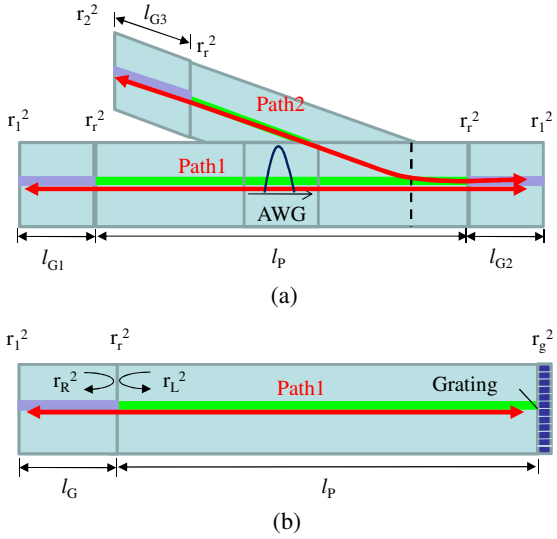

Fig. 2. Structures used for device analysis. (a) the detailed model (for steady-state analysis). Light passes the AWG (filter) passband twice during a round trip in the cavity. $l_{G(1,2,3)}$ and l_P indicate the lengths of the gain and passive sections. r_1^2 and r_2^2 are the reflectivities at the HR- and AR-coated facets. r_r^2 is the residual reflectivity at the interfaces between the gain and passive sections. (b) the simplified equivalent model (for steady-state and stability analysis). The grating to the right facet provides filtered optical feedback over a small range of frequencies. r_R^2 and r_L^2 are the right and the left effective reflectivities seen at the interface. r_g^2 is the grating peak reflectivity.

#118015 - $15.00 USD Received 1 Oct 2009; revised 8 Nov 2009; accepted 16 Nov 2009; published 30 Nov 2009

Table 1. Device parameters

Parameter	Value	Description
dg/dN	3.5×10^{-17} cm^{-2}	Linear differential gain
N_0	1.7×10^{18} cm^{-3}	Transparent carrier density
α_i	16 cm^{-1}	Internal loss
α_p	4 dB/cm	a-Si waveguide propagation loss
α_{AWG}	4 dB	AWG insertion loss
$\Delta\lambda_{AWG}$	0.6 nm	AWG passband width
ρ_{sp}	3 dB	Y-branch (splitter) loss
$l_{G1}/l_{G2}/l_{G3}$	1.15/1.15/1.7 mm	Gain section lengths
$l_{p1}/l_{p2}/l_{p3}/l_{p4}$	5/4.5/0.5/3 mm	a-Si waveguide lengths
r_1^2	90 %	Reflectivity at the HR-coated facet . r_r^2 and r_g^2 are the
r_2^2	0.01 %	Reflectivity at the AR-coated facet
r_r^2	0.01 %	Residual reflectivity at the interfaces
dg/dP	-3.6×10^{-6} cm^{-1}	Gain saturation factor
n_{0G}	3.2	Effective refractive index of gain sections without the carrier densities
n_P	3.2	Effective refractive index of a-Si waveguide
α	4	Linewidth enhancement factor

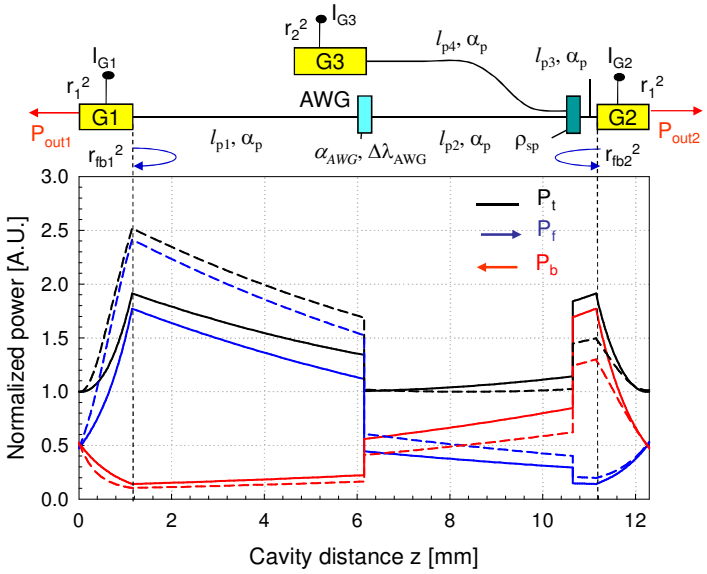

Fig. 3. Calculated normalized power distributions of the lasing mode with the lowest threshold gain along the path 1 under the current condition 1 (I_{G1}/ I_{G2}/I_{G3} = 38.6/38.6/0mA, solid lines) and the condition 2 (80/60/0mA, dashed lines). The blue, the red, and the black line indicate the forward P_f, the backward P_b, and the total power P_t (= P_f + P_b), respectively. r_{fb1}^2 and r_{fb2}^2 are the feedback power ratio at the right facet of the gain 1 and at the left facet of the gain 2. In this calculation model, AWG loss and Y-branch loss, α_{AWG} and ρ_{sp}, appear at the certain positions, z = l_{G1}+l_{p1} (= 6.15mm) and l_{G1}+l_{p1}+l_{p2} (= 10.55mm), respectively.

#118015 - $15.00 USD Received 1 Oct 2009; revised 8 Nov 2009; accepted 16 Nov 2009; published 30 Nov 2009

The device has an asymmetric structure along the path 1 but the output powers, P_{out1} and P_{out2}, are identical regardless of the current conditions owing to the same facet reflectivity r_1^2. Besides, the power distributions within the gain section 1 and 2 are symmetric under the condition 1 (solid lines) while asymmetric distributions appear under the condition 2 (dashed lines) due to the current difference between the gain sections. The feedback power ratios, r_{fb1}^2 (= P_b (z = l_{G1}) / P_f (l_{G1})) and r_{fb2}^2 (= P_f (l_T-l_{G2}) / P_b (l_T-l_{G2}), l_T is the total cavity length), are 8 % and 8 % for condition 1 and 4.3 % and 15.1 % for condition 2, respectively. These values will be used as the grating peak reflectivity r_g^2 (Fig. 2(b)) in mode stability analysis.

Mode stability can be determined by finding the location of the poles (zeros in [11]) on the Laplace-plane (complex frequency = $f + j\sigma$) in the small-signal transfer function (determinant) of external-cavity system. The modes in the cavity (path 1) are found by solving the steady-state condition. The poles correspond to small-signal oscillations of the considered mode, whose imaginary part σ represents the damping. If one of the poles has a negative imaginary part, the oscillation is diverged and the mode is unstable; otherwise the mode is stable. In mode stability analysis, the first model was rather inappropriate due to the complicated structure and coupled-cavity effect [14] caused by at least two gain sections. Instead of it, we utilized the simplified structure shown in Fig. 2(b) under the following conditions: no light generation from the path 2 (zero injection current to gain section 3), neglect of coupled-effect between both gain sections in path 1 (the effect of individual gain section on the mode stability is treated independently), and no consideration of longitudinal spatial hole-burning and spectral gain curvature in gain section.

In order to check the stability of the modes obtained from the steady-state condition, the poles should satisfy the following equation [11]:

$$D(\tilde{\omega}) = (X + B)(X' + B') - BB' = 0 \tag{1}$$

with

$$\begin{aligned} &X = 1 - G(\tilde{\omega}) \quad X' = 1 - G^*(-\tilde{\omega}) \\ &B = B(\tilde{\omega}) \qquad B' = 1 - B^*(-\tilde{\omega}) \\ &G(\tilde{\omega}) = \frac{r_R(\omega_s + \tilde{\omega})}{r_R(\omega_s)} e^{-j\tilde{\omega}\tau_{in}} \\ &B(\tilde{\omega}) = \frac{1 - e^{-j\tilde{\omega}\tau_{in}}}{2j\tilde{\omega}} \left\{ \frac{(1 + j\alpha)\left[\omega_R^2 + \frac{1}{4}(\Gamma_N - \Gamma_P)^2\right]}{j\tilde{\omega} + \Gamma_N} + \Gamma_P \right\} \end{aligned} \tag{2}$$

where D is the system determinant, $\tilde{\omega} = \omega - \omega_s$ is the complex angular frequency excursion from the steady-state frequency ω_s, τ_{in} is the internal cavity round-time (= $2l_G/v_g$, v_g is the group velocity), ω_R is the relaxation angular frequency (= $\sqrt{\gamma G_N P}$, $\gamma = v_g g$, $G_N = v_g dg/dN/V_c$, P the photon number, g is the modal gain, and V_c is the volume of the active region), Γ_N is the damping rate of the carrier density (= $\tau_s^{-1} + G_N P$, τ_s is carrier lifetime), and Γ_P is the damping rate of the photon density (= $-G_P P$, $G_P = v_g dg/dP$).

Stability was checked for all the modes near the grating peak (the grating peak reflectivity r_g^2 of 8% and the bandwidth of 40 GHz) with the injection current. Figures 4(a) and 4(b) show the detuning (stable) range and the minimum damping (minimum imaginary frequency of the poles) σ_{min} for the modes at the current of I_{th} + 70 mA for various gain section lengths. The stable range is getting larger with the decrease of the l_G. It was found that this is quite different from decreasing the passive length l_P. There exists the critical length (l_{Gc} ~ 700 μm) which determines if the stable range can be enlarged for frequencies lower than the grating

#118015 - $15.00 USD Received 1 Oct 2009; revised 8 Nov 2009; accepted 16 Nov 2009; published 30 Nov 2009

peak (zero detuning). From the result, it may be estimated that the previous structure [9, $l_{G1(2)}$ = 1.15 mm) would be operate at unstable range. When the l_G decreases, the peak of the σ_{min} is shifted toward lower frequency (longer wavelength) and its value is increased, as shown in Fig. 4(b). This means that the increase of σ_{min} (decrease of the gain section) can result in a higher side mode suppression ratio (SMSR). It can be explained by the fact that the damping of the poles is related to the threshold gain difference between the lasing and side modes. We have also checked the stability for the r_g^2 of 4 ~ 20% according to the feedback power ratios obtained in Fig. 3. There was little significant difference in the stable range and in the damping in comparison with the Fig. 4. It was found that with the increase of the r_g^2, the stable range is expanded by degree and the minimum damping is increased accordingly. We note here that for $l_G > l_{Gc}$, the r_g^2 can have a considerable influence on the mode stability at high current and, as a result, the same feedback power ratio can be preferred to minimize the influence by the relatively smaller feedback ratio.

Practically, the calculated l_{Gc} and σ_{min} can be changed by the variation of the parameters assumed in this simulation such as dg/dP, α-parameter, and filter bandwidth. Besides, they may be reduced or distorted by the consideration of the neglected effects including the residual reflections.

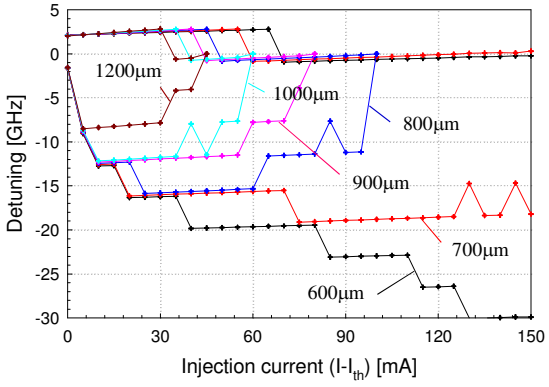

(a)

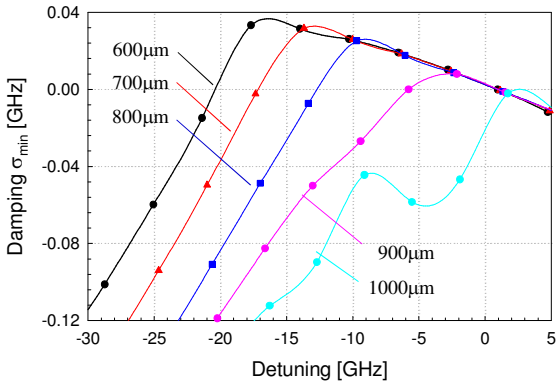

(b)

Fig. 4. (a). Stable ranges around the grating peak wavelength for increasing current above threshold I_{th} with respect to the length of the gain section l_G and (b) minimum damping σ_{min} for the modes at the current of I_{th}+70mA for various l_G. In (a), the boundaries of stable range were set to be the middle values between stable and unstable mode. The grating peak reflectivity r_g^2 of 8% and the bandwidth of 40 GHz were used. The interface reflection was neglected ($r_r^2 = 0$).

#118015 - $15.00 USD Received 1 Oct 2009; revised 8 Nov 2009; accepted 16 Nov 2009; published 30 Nov 2009

3. Experimental results

The whole configuration of the fabricated devices, as shown in Fig. 1, is similar to that of [9] but there are some differences in AWG design (free spectral range of 52 nm, channel spacing of 3.2 nm), structures of the gain section (six 7 nm-thick strained quantum wells and 2.5 μm-wide ridge waveguide) and a-Si waveguides (core refractive index of 3.36), and fabrication techniques (stepper process and dry-etching, etc.). The device size is 4.5 × 5.5 mm^2. By measuring individual components, propagation loss of 3 ~ 4 dB/cm was obtained for 3 μm-wide a-Si ridge waveguides deposited on thermally oxidized Si wafer, and -3 dB passband width of 0.6 nm and the crosstalk level of about 28 dB for a-Si AWG with the width of 2 μm. For a-Si waveguides deposited on InP substrates, however, propagation losses of more than 5 dB and additional bending losses of about 1.5 dB were obtained. We think this is mainly due to the a-Si film blisters.

In order to examine the effect of the length of gain section for path 1 on the mode stability, we have used two different kinds of structures: for the sample 1, the l_{G1} and l_{G2} are 800 μm and 800μm and, for the sample 2, 600 μm and 350 μm, respectively. The uncoated samples were measured at the facet of the gain section 2 without the current of gain section 3 in order to remove the effect of the path 2. Figure 5 shows the measured output spectra of both samples under the same conditions.

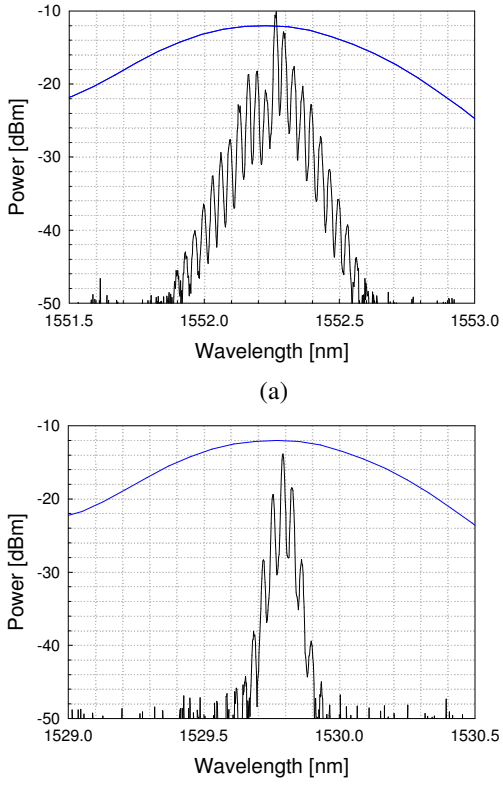

Fig. 5. Measured power spectra (black lines) of (a) sample 1 and (b) sample 2 under I_{G3} = 0 mA. Powers were obtained through the uncoated facet on the side of gain 2 at the currents (I_{G1} / I_{G2} =150 / 100 mA). Blue lines denote the spectral response of a-Si AWG. The resolution bandwidth is 0.01 nm [Ando AQ6317B].

#118015 - $15.00 USD Received 1 Oct 2009; revised 8 Nov 2009; accepted 16 Nov 2009; published 30 Nov 2009

Although they both have the same AWG passband, their spectra are quietly different. It is clearly shown that the spectral width of the sample 2 is narrower than that of the sample 1. We also confirmed the same result by reducing the gain part of the chip by step. Therefore, these experiment results show that the spectral width is highly dependent on the length of the gain medium. It can be thought that the spectral narrowness is mainly attributed to the increase of side-mode damping which results in a higher SMSR according to Fig. 4. However, since the mode suppression between the central mode and the adjacent modes is still low for both samples, there is little significant difference between them in SMSR. For this result, we think both samples may have not enough stability (σ_{min}) to suppress the adjacent modes (see Fig. 3 in [11], in complex frequency curve the lower curve of the coupled side modes is changed U-shape to double W-shape as the stability becomes improved). This can be explained that in external-cavity system the relatively high passive waveguide loss reduces the feedback power from the grating, and therefore, this power reduction makes weakened the side-mode damping originated from the gain saturation effect. Since this high passive loss can be somewhat compensated by reducing the mirror loss, the sample 2 was measured again after the HR coating. The improvement of about 10dB in SMSR at the same condition was obtained as expected. Figure 6 shows the measured output powers of (a) the sample 2 after the HR-AR coatings and (b) the packaged MFL chip of which structure is the same as the [9] (provided by Novatronix co).

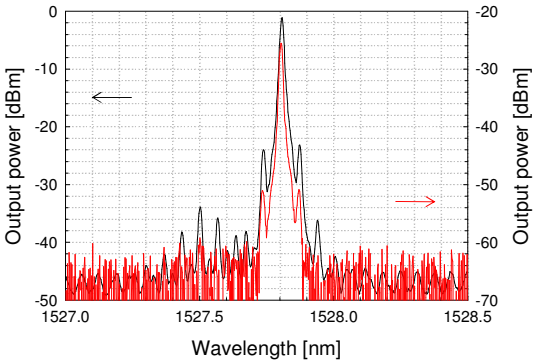

(a)

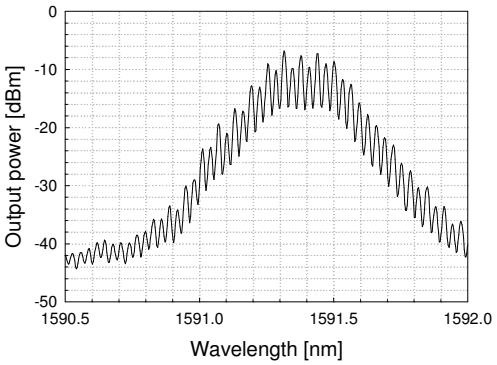

(b)

Fig. 6. Measured output power spectra of (a) the sample 2 after the coatings and (b) the packaged chip [9]. Output powers (black lines) were measured through the AR-coated facet on the side of gain 3 at $I_{G1}/I_{G2}/I_{G3}$ =140/65/180mA for (a) and at 100/50/100mA for (b). The red line in (a) is the measured spectrum at the HR-coated facet on the side of gain 2 at 100/65/180mA. The resolution bandwidth is 0.01 nm.

#118015 - $15.00 USD Received 1 Oct 2009; revised 8 Nov 2009; accepted 16 Nov 2009; published 30 Nov 2009

A single mode with the SMSR of more than 22 dB (black line) appears for sample 2 while a multi-mode with a wide spectral width for the packaged chip. In sample 2, there was no difference between AR- and HR-coated facets in spectra except the power value. The SMSR was changed 15 dB to 30 dB with the combination of the operation current. It appeared that the maximum SMSR can be obtained when the current densities (= $I/l_{G1(2)}$) of the gain 1 and 2 are identical as shown in red-line of Fig. 6(a). This results from the same feedback power ratios.

4. Conclusion

We have demonstrated theoretically and experimentally that the dynamic mode stability can be significantly improved by simply reducing the length of the gain section in long-cavity lasers with an intra-cavity filter. Besides, we have implemented the monolithically integrated lasers with a-Si AWG with improved mode stability compared to its original device. This type laser can be used as a low cost OLT (optical line terminal) source in WDM-PON by modifying the schematics. Additional improvements for the low a-Si WG losses, the multiple operation, and small-size are the subject of the current investigations. These works realizing the structure with the improved performances are ongoing.

#118015 - $15.00 USD Received 1 Oct 2009; revised 8 Nov 2009; accepted 16 Nov 2009; published 30 Nov 2009